Supplement of The Cryosphere, 18, 4547–4565, 2024
https://doi.org/10.5194/tc-18-4547-2024-supplement

The Cryosphere
Open Access

Supplement of

A model framework for atmosphere–snow water vapor exchange and the associated isotope effects at Dome Argus, Antarctica – Part 1: The diurnal changes

Tianming Ma et al.

Correspondence to: Lei Geng (genglei@ustc.edu.cn)

S1. Meteorological data processing

At Dome A, air temperature measured at height z exhibits a harmonic on the diurnal scale (Ma et al., 2010). An interpolation method is thus used to make a continuous record of air temperature when observations are missed (e.g., Laepple et al., 2018). The formula for data interpolation is as follows:

$$T_a = T_{mean} + A1\cos(\omega t + \Phi) + A2\sin(\omega t + \Phi) \quad \text{(S1)}$$

where T_{mean} denotes the daily mean from temperature observations, A1 and A2 are the amplitude of the harmonics, ω and t is the angular frequency and time, Φ denotes the phase of first harmonics.

The raw data of relative humidity at height z is the relative humidity with respect to the water surface (RH_w), measured with the HMP35D humidity probe (Xiao et al., 2008; Ding et al., 2022). The RH_w can be expressed as a percentage:

$$RH_w = e_w / e_w^s \times 100\% \quad \text{(S2)}$$

where e_w is the water vapor pressure of air, and e_w^s is the saturated vapor pressure with respect to the water surface at the air temperature that can be calculated using the Clausius-Clapeyron equation. When calculating the effective fractionation factor (α_f) in the model (Eq: (15) in the main text), the RH_w needs to be converted as the relative humidity over ice at the temperature of the air (RH_i). The conversion between RH_i and RH_w is proposed based on the calibration procedures of Anderson et al. (1984) and Makkonen & Laakso (2005). The details are as follows: 1) The RH_w observations are firstly rescaled using the maximum RH_w of all measured values at each air temperature point (T_a):

$$RH_w' = RH_w(T_a) / RH_w^{max}(T_a) \quad \text{(S3)}$$

2) RH_w' values are then converted to RH_i using Eq: (S4):

$$RH_i = (e_w^s(T_a) / e_i^s(T_a)) \times RH_w' \quad \text{(S4)}$$

where e_i^s represents the saturated vapor pressure with respect to ice at the air temperature. Similar to e_w^s, e_i^s is also calculated by the Clausius-Clapeyron equation.

In addition, the relative humidity of the air with respect to the surface temperature (h) in Eq: (14) is also computed from RH_w observations. The first step for h calculations is the rescaling RH_w based on Eq: (S3), same to the RH_i conversion procedures. The second step is computing h with the saturated vapor pressure with respect to ice at the surface temperature (Eq: (S5)):

$$h = (e_w^s(T_a) / e_i^s(T_s)) \times RH_w' \quad \text{(S5)}$$

S2. Uncertainty analysis

At each time step, we first calculated the standard deviation as the uncertainties (1σ) of meteorological conditions (including wind speed, air temperature, relative humidity) by stacking the hourly observations of those selected days. Then, this stacking method was applied to determine the uncertainty of calculated surface temperature and the latent heat flux (Q_{LE}). The estimated uncertainties from stacking method were plotted in Figure 2 of the main text (shaded areas).

The uncertainties of simulated isotopic values (Q_δ) were calculated using two different methods. In the Dome C simulations, the uncertainties of water vapor and snow isotopes were calculated by stacking 11 diurnal variations of simulated results from January 5 to 16 in 2015 (as indicated by the shaded area in Figure 3). However, for Dome A simulation cases, the stacking method is not available for uncertainty estimation. This is because Dome A simulations under cloudy and clear-sky conditions are based on averaged meteorological conditions. Here we used error propagation method as an alternative solution, as referred to by Radić et al. (2017). The calculating steps are as follows: 1) we calculated the uncertainties of the fractionation coefficient (Q_α) based on the standard deviation of surface temperature (Eq: (S6)). 2) Q_δ were obtained using uncertainties of latent heat (Q_{LE}) and Q_α (Eq: (S7)).

$$Q_\alpha = \alpha' * Q_{Ts} \tag{S6}$$

$$Q_\delta = \sqrt{\left(\frac{\partial\delta}{\partial\alpha} * Q_\alpha\right)^2 + \left(\frac{\partial\delta}{\partial LE} * Q_{LE}\right)^2} \tag{S7}$$

where α' is the derivative of fractionation coefficient (Eq:(13) of the main text), the $\frac{\partial\delta}{\partial\alpha}$ and $\frac{\partial\delta}{\partial LE}$ represents the derivative of fractionation coefficient and latent heat flux in the equation of isotopic balance of the model (Eq: (10) of the main text). The calculated uncertainties following propagation method are shown in the Figures 4-6 of the main text.

S3. The estimation of the initial value of the snow isotopic composition ($\delta^{18}O_{s0}$)

For non-summer seasons, the isotopes of precipitation were estimated using the regression line (slope of 0.64±0.02, R^2=0.59) of the non-summer precipitation isotopic composition and near surface air temperature at Dome F, Vostok and Dome C compiled by Pang et al. (2019). In summer, the R^2 of the correlation coefficient in summer is indeed small (0.13). To justify the estimate, in the revised manuscript, we also utilized the ECHAM5-wiso simulation data (Werner et al., 2011) which simulated precipitation isotopes according to temperature and other parameters. The comparison for these two calculations is shown in Fig. S1. It is clearly found that the results of the two methods agree with each other reasonably.

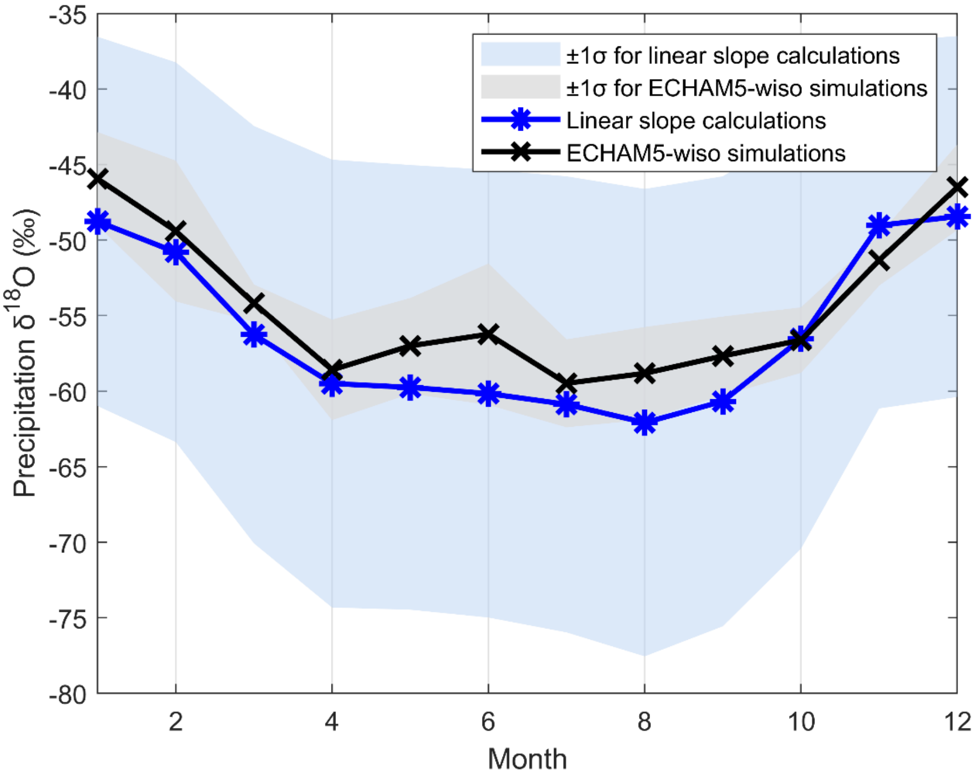

Figure S1: The estimated precipitation $\delta^{18}O$ and its standard deviation during the period of 2005-2011. Blue solid line with star marks represents the calculations using the temperature-isotope slope according to data from Pang et al. (2019), and the light blue shaded area is the uncertainties. Black solid line with x marks and light grey shaded area displays the ECHAM5-wiso simulation data and its uncertainties, respectively.

S4. The water vapor exchange between the boundary layer and the free atmosphere

In the model structure, we considered how mixing between the boundary layer and the free atmosphere can affect the water vapor isotopic composition in the near-surface atmospheric layer and snow isotopes. There is no doubt that mixing can occur under unstable atmospheric conditions with negative Richardson numbers (Ri<0). However, Zilitinkevich et al. (2008) also pointed out that such mixing does exist when Ri ranges between 0 and 0.1. To test the relationship between mixing occurrence conditions and Richardson numbers, we ran simulations for Dome C taking into account mixing when Ri<0.1 (Case I) and Ri<0 (Case II). The results are shown in Fig. S2. It is found that the simulations in Case I matches well with the observations (Casado et al., 2016). Also, the simulations in Case II are much lower than those in Case I, especially in the cooling time. Through this comparison, we incorporated mixing into the modeling once Ri<0.1.

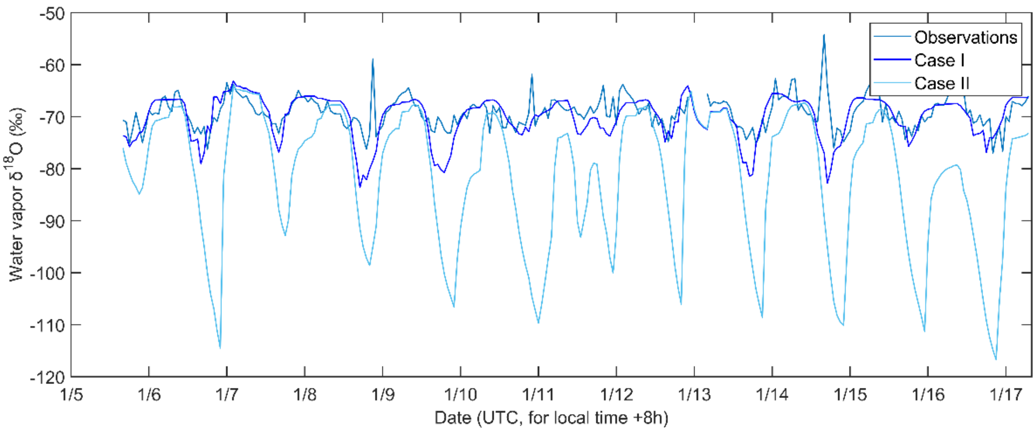

Figure S2: The comparison of water vapor isotopic composition between the simulated and observed changes at Dome C. Two simulated cases are presented here to discuss the occurrence condition of mixing between the boundary layer and the free atmosphere. In case I, the mixing is assumed to only happen when Ri<0 in the cooling phase, while case II also considers the occurrence of mixing when Ri<0.1 in the cooling phase.

S5. The sensitivity tests for other parameters

Besides the temperature and humidity, we also evaluated the effect of wind speed on simulations during atmosphere-snow water vapor exchange. A case simulation was designed for Dome A site and run for a 24-h period, with the averaged wind speed of 4m/s (Case II) higher than the mean value of those observations (Case I). The results are displayed in Fig. S3. It is found that the simulations with stronger wind show more significant diurnal variations in water vapor isotopes and snow isotopes. This difference suggests that strong variability in wind speed will enlarge the variations in latent heat, leading to a more significant diurnal change in water vapor isotopes and snow isotopes.

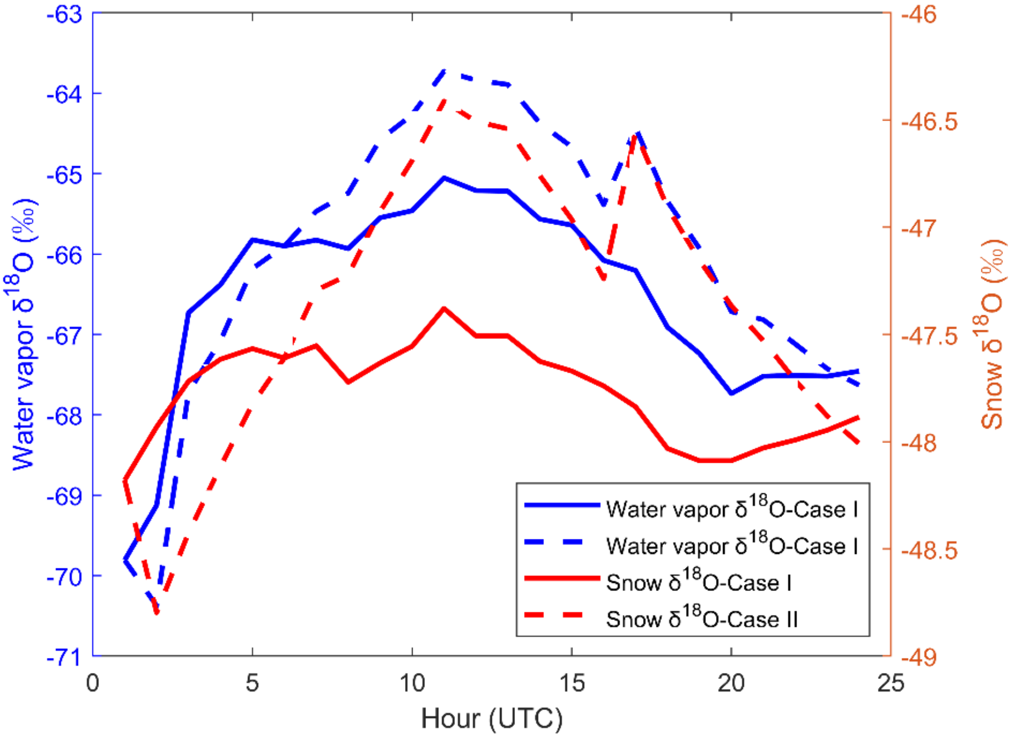

Figure S3: The comparison of water vapor isotopic composition between two simulated cases at Dome A. The simulations in two cases were driven using the averaged wind speed (Case I) and the strong diurnal changes in wind speed (Case II).

In addition, changes in surface roughness (z_0) might influence the isotopic effects of atmosphere-snow water vapor exchange (Vignon et al., 2017). Thus, we also design the sensitivity tests for z_0 and run for a 24-h period under summer clear-sky conditions at Dome A. The tests were focused on the sensitivity of surface snow and water vapor $\delta^{18}O$ to varying z_0 between 0.01 to 10 mm. All other simulation settings were the same as in Section 2.2.4 of the main text. The results of sensitivity tests for z_0 are shown in Fig. S4. As shown in the figures, the magnitude of the diurnal variations in water vapor $\delta^{18}O$ ($\delta^{18}O_v$) is very sensitive to z_0 (Fig. S4a) because z_0 determines the latent heat flux. The magnitude of diurnal variations in snow $\delta^{18}O$ ($\delta^{18}O_s$) is also sensitive to z_0 (Fig. S4b and S4c). However, the changes in $\delta^{18}O_s$ are smaller than $\delta^{18}O_v$.

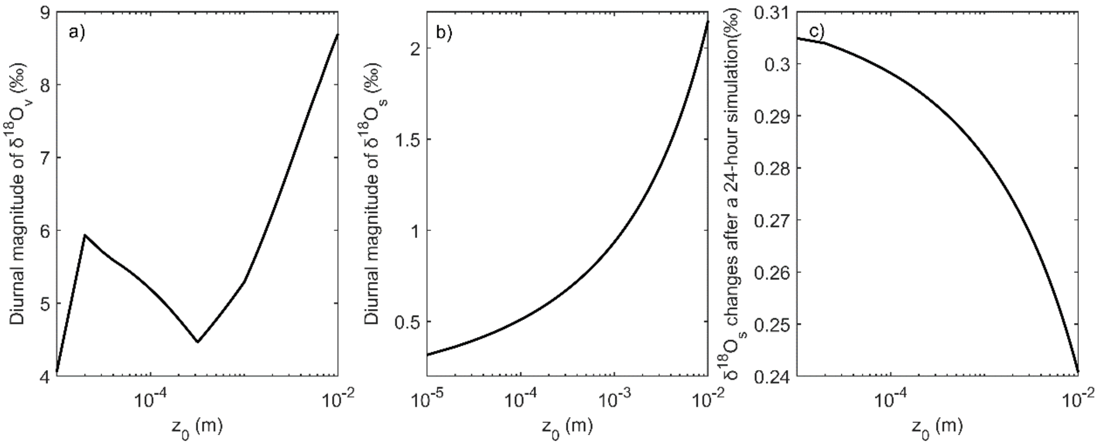

Figure S4: Sensitivity of the modeled results under Dome A clear-sky condition to changes in z_0. Panel S4a-S4c displays the modeled magnitude of $\delta^{18}O$ diurnal variations in water vapor ($\delta^{18}O_v$), the modeled magnitude of $\delta^{18}O$ diurnal variations in surface snow ($\delta^{18}O_s$), and $\delta^{18}O_s$ differences between the ending and starting values.

Table S1. List of variables in the model

Variables	Description (Unit)
Ex	Atmosphere-snow exchange flux ($kg \cdot m^{-2} \cdot s^{-1}$)
LE	Latent heat ($W \cdot m^{-2}$)
ρ_a	Dry air density ($kg \cdot m^{-3}$)
T_a	Air temperature at the reference height (K)
P_a	Atmospheric pressure (hPa)
L_s	Sublimation heat constant ($J \cdot kg^{-1}$), $L_s = 2.86 \times 10^6\ J \cdot kg^{-1}$
z	Reference height in the boundary layer (m), z = 4m at Dome A
q_a	Specific humidity of air ($kg \cdot kg^{-1}$)
q_s	Saturated specific humidity over ice surface derived from the Clausius-Clausius equation ($kg \cdot kg^{-1}$)
RH	Observed relative humidity (%)
RH_i	Calibrated relative humidity over ice surface (%)
S	unit area (m^2)
C_E	Transfer coefficient for humidity
u_a	Wind speed at the reference height ($m \cdot s^{-1}$)
k	von-karman constant, k=0.40
z_0	Surface roughness length for humidity exchange (m), $z_0 = 2.44 \times 10^{-4}$ m at Dome A
Ψ_M	Diabatic corrections with respect to the ratio of the reference layer height
L	Monin-Obukhov length (m)
$\bar{\theta}$	Mean potential temperature between the surface and a reference height in the boundary layer (K)
θ	potential temperature at the snow surface (K)
θ_z	potential temperature at the reference height (K)
u*	Friction velocity ($m \cdot s^{-1}$)
θ*	Temperature turbulent scale (K)
g	Gravity acceleration ($m \cdot s^{-2}$), g=9.8 m/s^2
Ri	Richardson number
M_s	Snow mass (kg)
M_v	Water vapor mass in the near-surface atmospheric layer (kg)
M_f	Water vapor mass exchanges between the near-surface atmospheric layer and the free atmospheric layer (kg)
ρ_s	Snow density ($kg \cdot m^{-3}$)
h_0	Snow height at initial time (m)
H_0	Near-surface boundary height at initial time (m)
R_s	Ratio between the abundance of heavy isotopes (^{18}O and D) and light isotopes (^{16}O and H) in the snow reservoir
R_v	Ratio between the abundance of heavy isotopes (^{18}O and D) and light isotopes (^{16}O and H) in the near-surface atmospheric water vapor reservoir
R_f	Ratio between the abundance of heavy isotopes (^{18}O and D) and light isotopes (^{16}O and H) in the free atmospheric water vapor reservoir
R_{Ex}	Ratio between the abundance of heavy isotopes (^{18}O and D) and light isotopes (^{16}O and H) in atmosphere-snow vapor exchange flux
S	Per unit surface area (m^2)
δ	Another denotation of isotopic ratio (‰)
δs_0	Snow isotopic composition at initial time (‰)
δv_0	Water vapor isotopic composition in the near-surface atmospheric layer at initial time (‰)
δf_0	Water vapor isotopic composition in the free atmospheric layer at initial time (‰)
k'	Diffusion coefficient
α_f	Efficient fractionation coefficient
α_e	Equilibrium fractionation coefficient
α_k	Kinetic fractionation coefficient
$D_i/D_{i'}$	Ratio between the molecular diffusivity of major and minor water isotopic species
σ	Stefan–Boltzmann constant ($W \cdot m^{-2} \cdot K^{-4}$), $\sigma = 5.67 \times 10^{-8}\ W \cdot m^{-2} \cdot K^{-4}$
ϵ	snow emissivity, ϵ =0.93 at Dome A, ϵ =0.99 at Dome C
LW_{dn}	Downward longwave radiative fluxes ($W \cdot m^{-2}$)
LW_{up}	Upward longwave radiative fluxes ($W \cdot m^{-2}$)

Reference

Anderson, P. S.: A Method for Rescaling Humidity Sensors at Temperatures Well below Freezing, Journal of Atmospheric and Oceanic Technology, 11(5), 1388-1391, doi: 10.1175/1520-0426(1994)011<1388:AMFRHS>2.0.CO;2, 1994.

Casado, M., Landais, A., Masson-Delmotte, V., Genthon, C., Kerstel, E., Kassi, S., Arnaud, L., Picard, G., Prie, F., Cattani, O., Steen-Larsen, H. C., Vignon, E., and Cermak, P.: Continuous measurements of isotopic composition of water vapour on the East Antarctic Plateau, Atmospheric Chemistry and Physics, 16(13), 8521-8538, doi: 10.5194/acp-16-8521-2016, 2016.

Ding, M., Zou, X., Sun, Q., Yang, D., Zhang, W., Bian, L., Lu, C., Allison, I., Heil, P., and Xiao, C.: The PANDA automatic weather station network between the coast and Dome A, East Antarctica, Earth System Science Data, 14, 5019–5035, doi: 10.5194/essd-14-5019-2022, 2022.

Hughes, A. G., Wahl, S., Jones, T. R., Zuhr, A., Hörhold, M., White, J. W. C., and Steen-Larsen, H. C.: The role of sublimation as a driver of climate signals in the water isotope content of surface snow Laboratory and field experimental results, The Cryosphere, 15(10), 4949-4974, doi: 10.5194/tc-15-4949-2021, 2021.

Makkonen, L., and Laakso, T.: Humidity Measurements in Cold and Humid Environments, Boundary-Layer Meteorology, 116(1), 131-147, doi: 10.1007/s10546-004-7955-y, 2005.

Ma, Y., Bian, L., Xiao, C., Allison, I., and Zhou, X.: Near surface climate of the traverse route from Zhongshan Station to Dome A, East Antarctica, Antarctic Science, 22(4), 443-459, doi: 10.1017/s0954102010000209, 2010.

Laepple, T., Münch, T., Casado, M., Hoerhold, M., Landais, A., and Kipfstuhl, S.: On the similarity and apparent cycles of isotopic variations in East Antarctic snow pits, The Cryosphere, 12(1), 169-187. doi: 10.5194/tc-12-169-2018, 2018.

Pang, H., Hou, S., Landais, A., Masson-Delmotte, V., Jouzel, J., Steen-Larsen, H. C., Risi, C., Zhang, W., Wu, S., Li, Y., An, C., Wang, Y., Prie, F., Minster, B., Falourd, S., Stenni, B., Scarchilli, C., Fujita, K., and Grigioni, P.: Influence of Summer Sublimation on δD, δ18O, and δ17O in Precipitation, East Antarctica, and Implications for Climate Reconstruction from Ice Cores, Journal of Geophysical Research: Atmospheres, 124(13), 7339-7358, doi: 10.1029/2018JD030218, 2019.

Radić, V., Menounos, B., Shea, J., Fitzpatrick, N., Tessema, M. A., and Déry, S. J.: Evaluation of different methods to model near-surface turbulent fluxes for a mountain glacier in the Cariboo Mountains, BC, Canada, The Cryosphere, 11, 2897–2918, doi: 10.5194/tc-11-2897-2017, 2017.

Ritter, F., Steen-Larsen, H. C., Werner, M., Masson-Delmotte, V., Orsi, A., Behrens, M., Birnbaum, G., Freitag, J., Risi, C., and Kipfstuhl, S.: Isotopic exchange on the diurnal scale between near-surface snow and lower atmospheric water vapor at Kohnen station, East Antarctica, The Cryosphere, 10(4), 1647-1663, doi: 10.5194/tc-10-1647-2016, 2016.

Vignon, E., Genthon, C., Barral, H., Amory, C., Picard, G., Gallée, H., Casasanta, G., and Argentini, S.: Momentum- and Heat-Flux Parametrization at Dome C, Antarctica: A Sensitivity Study, Boundary-Layer Meteorology, 162(2), 341-367, doi: 10.1007/s10546-016-0192-3, 2017.

Werner, M., Langebroek, P. M., Carlsen, T., Herold, M., and Lohmann, G.: Stable water isotopes in the ECHAM5 general circulation model: Toward high-resolution isotope modeling on a global scale, Journal of Geophysical Research: Atmosphere, 116, D15109, doi: 10.1029/2011jd015681, 2011.

Xiao, C., Li, Y., Allison, I., Hou, S., Dreyfus, G., Barnola, J. M., Ren, J., Bian, L., Zhang, S., and Kameda, T.: Surface characteristics at Dome A, Antarctica: first measurements and a guide to future ice-coring sites, Annuals of Glaciology, 48, 82–87, doi: 10.3189/172756408784700653, 2008.